Title	Nonlinear waves in Flagella(Mathematical Topics in Biology)
Author(s)	Murase, Masatoshi
Citation	数理解析研究所講究録 (1993), 827: 112-133
Issue Date	1993-03
URL	http://hdl.handle.net/2433/83290
Right	
Type	Departmental Bulletin Paper
Textversion	publisher

数理解析研究所講究録
第827巻 1992年 112-133

Nonlinear waves in Flagella

村瀬雅俊 (Masatoshi Murase)

Division of Information Dynamics
Tokyo Metropolitan Institute of Gerontology
35-2 Sakaecho, Itabashi-ku, Tokyo 173, Japan

A flagellum swimming in a viscous medium is modelled by a one-dimensional array of opposed-active elements. The resultant model is mathematically described by a forth-order partial differential equation. In the model, the active element is characterized by both *hysteresis* and *excitability* with respect to the sliding motion between the filaments. Hysteresis means that the element is either turned "on" or "off", depending on the history of the sliding motion. Excitability is defined when *active* sliding is triggered by *passive* sliding over a threshold. Combination of these properties leads to a spatio-temporal sliding pattern within the flagellar system, which in turn causes a bending pattern. Numerical simulations for the present model reveal that (i) *intrinsic* instability arises from this model system, (ii) the direction of propagating waves is reversed, (iii) such direction-reversing propagating waves are replaced by unidirectional waves after the insertion of a passive region at one end, and (iv) the increase in the system size leads to the chaotic behavior.

1. Introduction

Flagella are hair-like projections which are found on eukaryotic cells*. Their primary function is to move single cells through a fluid for locomotion. Most flagella show regular base-to-tip bend propagation[1] as illustrated in Figure 1. However, others show quite complex dynamical behavior such as the reversal of the direction of propagating waves[2-4], collision of waves which travel in the opposite directions[4-5], *intermittent* movements with *stopping* and *starting* transients[6], co-existence of different waves on different sections of a long insect flagellum[7].

Surprisingly, there is no essential difference in the structure of these flagella. The problem is, thus, to clarify the underlying mechanism leading to various modes of complex behavior. Although

* Confusingly, bacterial flagella share the same name as those of eukaryotes. They are, however, completely different in the structure and function.

many theoretical studies have been performed, they have focused on the regular base-to-tip bend propagation only[8-16]. No attempt has been made to understand the potentially important complex behavior.

In the present paper, I will solve the above problem based on recent theoretical studies[17-21].

2. The sliding filament mechanism

It is now established that bending waves in flagella are caused by the sliding filament mechanism[22-24]. Although actual flagella have nine outer microtubules[25], they are approximated by a two-filament system on the assumption that bending occurs in a single plane. As illustrated in Figure 2, bending does not occur when any parts of filaments slide equally (Fig.2B). If, however, sliding is restricted on local regions, bending is generated between the sliding and non-sliding region (Fig.2C). For such bending to be reversed, the direction of sliding must be reversed (Fig.2D). The flagellar system is, thus, modelled by a one-dimensional array of opposed-active elements, each of which has its own "preferred" direction.

3. Derivation of the basic equation

An arc length, s, is introduced to measure the distance along the flagellum from the base. Then, the sliding displacement, σ, is defined as a function of time, t, and space, s. Under the condition that sliding is restricted on local regions, we can assume that the sliding displacement, σ, is proportional to the bending angle, θ, between a horizontal axis and a line tangent to the flagellum. Once σ is specified, we can easily obtain the flagellar shape by the simple integration (cf. Fig.4). For convenience, σ is defined as a dimensionless sliding displacement and is allowed to vary between 0 and 1.

The moment-balance equation for a flagellum is written by

$$M_V + M_S + M_E = 0 \qquad (1)$$

where M_V, M_S and M_E are the external viscous, internal shear and internal elastic moments, respectively. To obtain the basic equation, let us specify each moment in equation (1).

Firstly, the external viscous moment, M_V, is given by the external viscous force, F_N [16]:

$$\frac{\partial M_V}{\partial s} + F_N = 0 . \qquad (2)$$

The external viscous force, F_N, in turn obeys the following force-balance equation [26]:

$$\frac{\partial F_N}{\partial s} + C_N V_N = 0 \qquad (3)$$

where C_N and V_N are normal components of the external viscous drag coefficient and the velocity, respectively. In equations (2) and (3), inertial terms are ignored because *Reynolds* numbers of flagella are extremely small. The normal component of the velocity, V_N, is, then, specified under the condition of continuation:

$$\frac{\partial V_N}{\partial s} = \frac{\partial \sigma}{\partial t} . \qquad (4)$$

In equations (3) and (4), translational movements of the flagellum as a whole is neglected based on the small-amplitude assumption[7]. This simplifies the algebra and the essential results should not be affected[16].

Secondly, the internal shear moment, M_S, is defined by the internal shear force, S [8]:

$$\frac{\partial M_S}{\partial s} = S . \qquad (5)$$

Lastly, the internal elastic moment, M_E, is proportional to the curvature:

$$M_E = E_B \frac{\partial \sigma}{\partial s} \qquad (6)$$

where E_B is the bending resistance.

Combining the above equations, we obtain the following basic equation:

$$C_N \frac{\partial \sigma}{\partial t} + \frac{\partial^2 S}{\partial s^2} + E_B \frac{\partial^4 \sigma}{\partial s^4} = 0 . \qquad (7)$$

4. The model

The problem is how to specify the internal shear force, S, in such a way that equation (7) gives rise to various modes of wave phenomena. In the present model, the internal shear force, S, is defined as follows:

$$S = F_I n_I + F_{II} n_{II} - K_e(\sigma - 0.5) - \gamma \frac{\partial \sigma}{\partial t} \qquad (8a)$$

$$F_I = Q(\sigma - 0.1)(\sigma - 0.3)(1 - \sigma) \qquad (8b)$$

$$F_{II} = Q(\sigma - 0.9)(\sigma - 0.7)(- \sigma) \qquad (8c)$$

$$n_I = \begin{cases} 1 & 0 < s \leq 0.2 \\ 0 & 0.2 < s < 1 \end{cases} \quad \text{(if initially } n_I = 0 \text{ for } \sigma > 0.2) \qquad (8d)$$

$$n_I = \begin{cases} 1 & 0 < s < 0.8 \\ 0 & 0.8 \leq s < 1 \end{cases} \quad \text{(if initially } n_I = 1 \text{ for } \sigma < 0.8) \qquad (8e)$$

where F_I and F_{II} are two opposing force-distance functions, n_I and n_{II} are two switching functions**, K_e the force constant of the passive elastic component, and γ the internal viscous resistance. In the following simulations, γ is taken to be zero except for Section 5.1 because it is negligible in experimental conditions[16]. Excitability is represented by equations (8b) and (8c), where Q is their force constant. See Figure 3A for details. Hysteresis is represented by equations (8d) and (8e). To avoid the competition between the two opposing elements, it is assumed that $n_I + n_{II} = 1$. See Figure 3B for details.

** Subscripts I and II indicate two opposing subsystems I and II, respectively.

Equations (7) and (8) are solved on the assumption that moments and forces vanish at both ends. These free-end boundary conditions are:

$$\left.\frac{\partial \sigma}{\partial s}\right|_{s=0,L} = \left.\frac{\partial^2 \sigma}{\partial s^2}\right|_{s=0,L} = 0 \qquad (9)$$

where L is a length of a model system.

5. Simulation results

5.1 Intrinsic instability

Although the internal viscous resistance, γ, has been considered to be negligible, large values of γ are empirically introduced to stabilize the wavelength of simulated waves in some models[10, 17]. This section investigates the effect of changing the ratio between the internal viscous resistance, γ, and the external viscous drag coefficient, C_N, on the stability of solutions to equations (7) and (8). For this purpose, three sets of values of γ and C_N are used: (i) γ = 50 pNms/24 nm, C_N = 0; (ii) γ = 50 pNms/24 nm, C_N = 0.5 pNms/μm^2; and (iii) γ = 0, C_N= 5 pNms/μm^2. A 50-μm long model flagellum is set to be *homogeneous* along the length of the system except that forced periodic oscillations are applied at one end in order to generate propagating waves.

Figure 4 shows the simulation results. In each case, the sliding displacement, σ, is plotted against space, s, in the left, and the corresponding bending pattern is shown in the right. The time interval between the two successive patterns is 5 ms. As the ratio of γ/C_N is decreased, the sliding pattern is deformed in two ways (see left panels) though its corresponding bending pattern does not change so much (see right panels). First, the plateau phases of the sliding pattern become spiky at local regions. Since spiky regions are localized, they are caused by the second-order space derivative

term in equation (7). Second, the plateau phases are globally inclined. These global changes result from long-range interactions which are described by the forth-order space derivative term in equation (7).

The system described by equation (7) is highly subjected to intrinsic instability when $\gamma = 0$ and $C_N = 5$ pNms/μm^2 (see Fig.4C). In the following simulations, solutions to equations (7) and (8) are obtained under these conditions as they are corresponding to the experimental conditions[18]. Because of the instability inherent in this model system, the dynamical behavior must be studied for long time. For this purpose, two types of representations are used. One is the *energy dissipation* which is obtained by integrating $(\partial\sigma/\partial t)^2$ with respect to space, s. This simply indicates the intrinsic instability. The other is a space-time diagram of σ in which the regions for $\sigma > 0.5$ are plotted by bars against space, s, at 5-ms time intervals. This plot reflects the spatio-temporal sliding pattern.

5.2 Reversal of propagating waves

A 50-μm long model flagellum has a homogeneous structure, in which opposed-active elements are arranged along the system from one end to the other. This model system is initially set to be straight except for the one end (i.e. the left end). Such an initial bend is developed and propagates toward the other end (i.e. the right end).

Figure 5A shows the energy dissipation. A number of spiky patterns exist which correspond to intrinsic instability. There are two minima in the time course of the energy dissipation: one is at t = 1120 ms and the other is at t = 2340 ms. Figure 5B shows the space-time diagram of σ. Waves which propagate toward the right are represented by successive bars moving in the rightward direction. As indicated by the first arrow at t = 1120 ms, the

direction of propagating waves is reversed. This reversal occurs as follows. The trailing edge of the original wave first slows down, while the leading edge does not significantly change its propagating velocity. Then, the wave changes its form and the deformed part sends out a wave which propagates in the direction opposite to the original direction (i.e. wave splitting[27]). This new wave collides with the subsequent wave. Since the new wave is large enough, it can destroy the other. As a result, there are only waves which propagate toward the left. The next reversal of these propagating waves occurs at t = 2340 ms as indicated by the second arrow.

If two waves which propagate in the opposite directions are identical, they pass through on collision[18]. Non-annihilating propagating waves of this kind are known as *solitons*. Non-annihilating waves are also observed in real flagella[4, 5].

5.3 Insertion of passive region at one end

The model system examined in the previous section demonstrated the reversal of propagating waves and soliton-like behavior. The problem still remaining is how to demonstrate unidirectional waves typical of "normal" flagella. To solve this problem, let us consider the fine structure of sea urchin sperm flagella which show the regular waves. These flagella are 41-43 μm long. Each flagellum has an inert *terminal piece* of 5-8 μm long at the distal end[7] and has a *basal plate* at the basal end[28]. Based on these observations, opposed-active elements are removed from the distal 10 μm of the 50-μm long model flagellum, and a strong elastic component is placed at the base. Mathematically, this situation is modelled when $Q = 0$ for $40 < s < 50$ μm and $K_e = 50$ pN/24 nm for $s = 1$ μm.

Figure 6A shows the energy dissipation. The peaks of spiky patterns are reduced extensively. The passive terminal region works like a bulk system which can absorb the instability arising from the active region. Figure 6B shows the space-time diagram of σ. As a result of the reduction of the intrinsic instability, only unidirectional propagating waves are demonstrated.

5.4 Increase in the system size

The model system is set to be homogeneous again, but its length is set to be 100 μm. A single propagating wave is initially present in the system. It propagates to the right and two waves are reflected at the right end based on the wave splitting mechanism (see Section 5.3). The first one is propagating slowly, while the second fast. Since the system size is doubled, the average value of the energy dissipation is almost doubled as indicated by Figure 7A. Figure 7B shows the space-time diagram of σ. As indicated by the first arrow, the second wave collides with the first one at t = 425 ms. After the collision, they continue to propagate. Collision of two waves which propagate in the same direction is experimentally observed. Following the collision, the system shows unidirectional propagating waves for a while. However, as indicated by the second arrow, the spatio-temporal sliding pattern begins to be chaotic at t = 1260 ms. There are different sections which show quite different wave parameters such as the wavelengths and wave frequencies. This chaotic behavior may correspond to the wave patterns observed in a long insect flagellum[7].

6. Discussion

The most important problem is how to specify the internal shear force, S, in such a way that equation (7) gives rise to various types of wave phenomena. In the present paper, the shear force, S,

was defined as a function of σ under the condition of $\gamma = 0$ in equation (8a) as in Sections 5.2 - 5.4:

$$S = S(\sigma) . \qquad (10)$$

It is very difficult to solve the above problem because the system described by equations (7) and (10) is subjected to the intrinsic instability. To understand this situation, let us consider a simple case that the internal shear force, S, is proportional to the sliding displacement, σ. Then, the second term in equation (7) corresponds to the *negative* diffusion leading to *destabilization*, while the third term causes *stabilization*. The competition between the two properties leads to intrinsic instability. Furthermore, there are only even powers of the space derivatives. This means that symmetry holds with respect to space, s; that is, the equation is invariant under the spatial inversion $s \rightarrow - s$. As a result, both distally propagating and proximally propagating waves were equally developed.

To get unidirectional waves, the structural asymmetry such as the terminal piece without active elements was taken into account. The passive region absorbed instability arising from the active region. The passive region in isolation does not show any function. But it can work to control orders when it coexists with the active region. By analogy with this model behavior, it is important to study any network systems (e.g. gene network, immune network, and nerve network) which involve non-active elements.

Besides the present model, two other types of models have been proposed in order to account for normal base-to-tip bend propagation: *curvature-controlled* models[8-9, 11-16] and *self-oscillatory* models[10]. Curvature-controlled models assume that the shear force, S, is defined as a function of the curvature, $\partial\sigma/\partial s$:

$$S = S\left(\frac{\partial\sigma}{\partial s}\right) . \qquad (11)$$

To understand the meaning of equation (10), let us consider a simple case that the shear force, S, is proportional to the curvature, $\partial\sigma/\partial s$. Then equation (7) does not hold the symmetry with respect to space, s, because of the presence of odd power of the space derivative. As a result, either distally or proximally propagating waves are present depending on the sign of the proportionality constant. However, once the sign of the constant is specified, these models can not account for two waves propagating in the opposite directions. Furthermore, there is no direct experimental evidence which supports equation (11).

Self-oscillatory models assume high internal viscosity, γ, to get unidirectional propagating waves. Here, the shear force, S, is conventionally represented as follows:

$$S = S - \gamma\frac{\partial\sigma}{\partial t} . \qquad (12)$$

Let us consider the extreme case of $C_N = 0$. Equation (7) can be reduced to the following reaction-diffusion equation:

$$\gamma\frac{\partial\sigma}{\partial t} = E_B\frac{\partial^2\sigma}{\partial s^2} + S. \qquad (13)$$

In this case, it is easy to get unidirectional propagating waves if an appropriate pace-maker is placed at one end of the system. However, the internal viscosity, γ, is generally considered to be negligible, which is inconsistent with equation (12). It is now clear that any models except for the present model are based on *ad hoc* assumptions to account for regular wave phenomena.

Intrinsic instability has not been discussed in the field of cellular motility. One reason for this is that theoreticians have focused on the regular behavior though there are experimental

observations for irregular modes of wave phenomena. Another reason is that it is very difficult to grasp the deformed patterns from the flagellar shape only (see right panels of Fig.4). For these reasons, the observed irregularity has been ascribed to *random noise*.

Equations similar to equation (7) have been discussed in different physical contexts. For example, the *Kuramoto-Sivashinsky* equation[29-31] and the *generalized reaction-diffusion* equation[32] have this class of intrinsic instability. Numerical simulations for these equations show complex dynamics. Despite the diversity of dynamical systems, it is very interesting to notice that there may be a common principle behind them. I hope that the present study stimulates the investigation of such a principle.

References

1) Gray, J. *J. Exp. Biol.* **32**, 775 (1955).

2) Goldstein, S. F., Holwill, M. E. J. and Silvester, N. R. *J. Exp. Biol.* **53**, 401 (1970).

3) Holwill, M. E. J. and McGregor, J. L. *Nature* **255**, 157 (1975).

4) Alexander, J. and Burns, R. G. *Nature* **305**, 313 (1983).

5) Holwill, M. E. J. *J. Exp. Biol.* **42**, 125 (1965).

6) Gibbons, I. R. *J. Musc. Res. Cell Motility* **7**, 245 (1986).

7) Rikmenspoel, R. *Biophys. J.* **23**, 177 (1978).

8) Brokaw, C. J. *J. Exp. Biol.* **55**, 289 (1971).

9) Brokaw, C. J. *Biophys. J.* **12**, 564 (1972).

10) Brokaw, C. J. *Proc. Nat. Acad. Sci. U.S.A.* **72**, 3102 (1975).

11) Brokaw, C. J. *Symp. Soc. Exp. Biol.* **35**, 313 (1982).

12) Brokaw, C. J. *Biophys. J.* **48**, 633 (1985).

13) Brokaw, C. J. In *Cell Movement Vol. 1*, eds. F. D. Warner, P. Satir and I. R. Gibbons, Alan R. Liss, New York, pp267 (1989).

14) Hines, M. and Blum, J. *Biophys. J.* **23**, 41 (1978).

15) Hines, M. and Blum, J. *Biophys. J.* **25**, 421 (1979).

16) Blum, J. and Hines, M. *Quart. Rev. Biophys.* **12**, 103 (1979).

17) Murase, M. and Shimizu, H. *J. Theor. Biol.* **119**, 409 (1986).

18) Murase, M, Hines, M. and Blum, J. *J. Theor. Biol.* **139**, 413 (1989).

19) Murase, M. *J. Theor. Biol.* **146**, 209 (1990).

20) Murase, M. *J. Theor. Biol.* **149**, 181 (1991).

21) Murase, M. *Dynamics of Cellular Motility*, Manchester University Press, Manchester (1992).

22) Summers, K. and Gibbons, I. R. *Proc. Nat. Acad. Sci. U.S.A.* **68**, 3092 (1971).

23) Sale, W. S. and Satir, P. Proc. *Nat. Acad. Sci. U.S.A.* **74**, 2045 (1977).

24) Satir, P., W-Steider, J., Lebduska, S., Nasr, A. and Avolio, J. *Cell Motility*, **1**, 303(1981).

25) Warner, F. D. In *Cilia and Flagella*, ed. by M. A. sleigh, Academic Press, London (1974).

26) Gray, J. and Hancock, G. J. *J. Exp. Biol.* **32**, 802 (1955).

27) Marek, M. and Sevcikova, H. In *Self-organization. Autowaves and Structures Far from Equilibrium.* ed. V. I. Krinsky, Springer-Verlag, Berlin (1984).

28) Sleigh, M. A. *The Biology of Cilia and Flagella.* Pergamon Press, Oxford (1962).

29) Kuramoto, Y. *Chemical Oscillations, Waves, and Turbulence.* Springer-Verlag. Berlin (1984).

30) Sivashinsky, G. I. *Acta Astronautica* **4**, 1177 (1977).

31) Manneville, P. In *Propagation in Systems Far from Equilibrium.* eds. Westreid, J. E., Brand, H. R., Manneville, P., Albinet, G., and Boccara, N. Springer-Verlag. Berlin, pp265 (1988).

32) Murray, J. D. *Mathematical Biology.* Springer-Verlag. Berlin (1989).

Figure Captions

Figure 1

Propagating waves typical of "normal" flagella. Successive waves (1 → 3) propagate toward the tip of a flagellum as indicated by the arrow.

Figure 2

Diagrams showing how sliding motion causes bending motion in a two-filament system. (A): The flagellum is straight and no bending occurs without sliding motion. (B): No bending is initiated when sliding occurs equally throughout the length of the flagellum. (C): If sliding is localized, bending occurs between the sliding and non-sliding regions. (D): When the direction of sliding is reversed, the flagellum bends in the direction opposite to the previous direction as shown in (C). The arrows indicate the directions of relative sliding.

Figure 3

The cubic force-distance and hysteresis switching functions. (A): F_I and F_{II} are represented by solid and dotted lines, respectively. They are defined as a function of the sliding displacement, σ. The force constant, Q, is taken as 250 pN. (B): The binary function is defined in the region $0.2 < \sigma < 0.8$. n_I and n_{II} give either the discrete values 0 or 1 under the condition of $n_I + n_{II} = 1$.

Figure 4

The sliding displacement, σ, as a function of the space, s, shown in the left, and the corresponding bending pattern shown in the right. The model flagellum is set to be homogeneous (Q = 250 pN and K_e = 1 pN/24 nm for $0 < s < 50$ μm) except that forced oscillations are

applied. The period of the oscillations is 60 ms. The flagellar shapes in the (x, y) coordinate are obtained by:

$$x(s) = \int_0^s \cos(\sigma - 0.5)ds, \qquad y(s) = \int_0^s \sin(\sigma - 0.5)ds .$$

Two successive patterns in each panel are shown at 5-ms time intervals. Parameters are: γ = 50 pNms/24 nm, C_N = 0 in (A); γ = 50 pNms/24 nm, C_N = 0.5 pNms/μm^2 in (B); and γ = 0, C_N= 5 pNms/μm^2 in (C).

Figure 5

The energy dissipation (A) and space-time diagram of σ (B). The flagellum is set to be homogeneous. Parameters are: γ = 0, C_N= 5 pNms/μm^2, Q = 250 pN and K_e = 1 pN/24 nm for 0 < s < 50 μm. Simulation results are shown up to t = 3000 ms.

Figure 6

The energy dissipation (A) and space-time diagram of σ (B). The flagellum is set to be inhomogeneous. Parameters are: γ = 0, C_N= 5 pNms/μm^2, Q = 250 pN and K_e = 50 pN/24 nm for s = 1 μm, Q = 250 pN and K_e = 1 pN/24 nm for 1 < s < 40 μm, and Q = 0 and K_e = 1 pN/24 nm for 40 < s < 50 μm. Simulation results are shown up to t = 2000 ms.

Figure 7

The energy dissipation (A) and space-time diagram of σ (B). The flagellum is set to be homogeneous. Parameters are: γ = 0, C_N= 5 pNms/μm^2, Q = 250 pN and K_e = 1 pN/24 nm for 0 < s < 100 μm. Simulation results are shown up to t = 2000 ms.

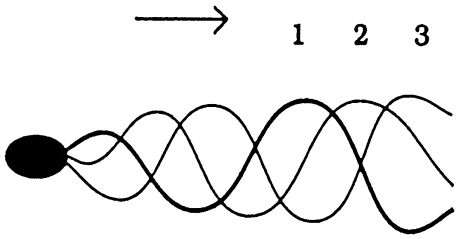

Fig. 1

Sliding Filament Mechanism

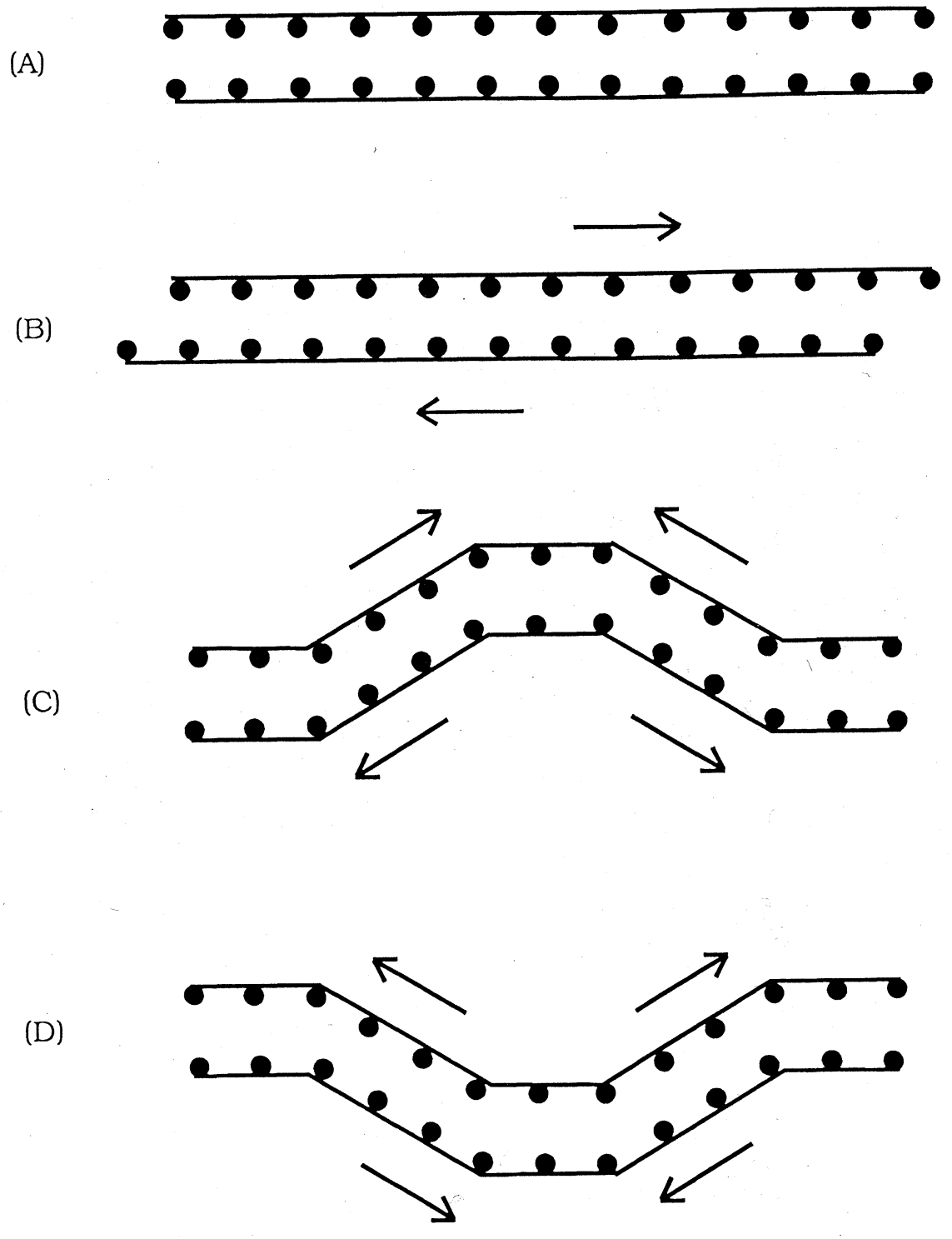

Fig.2

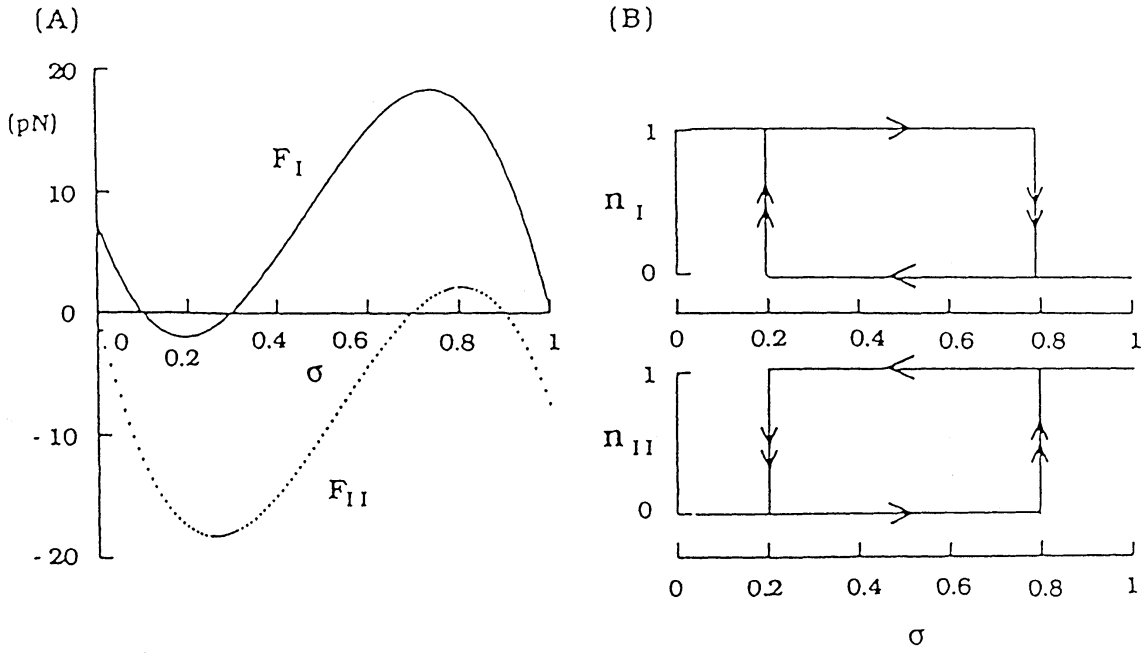

Fig 3

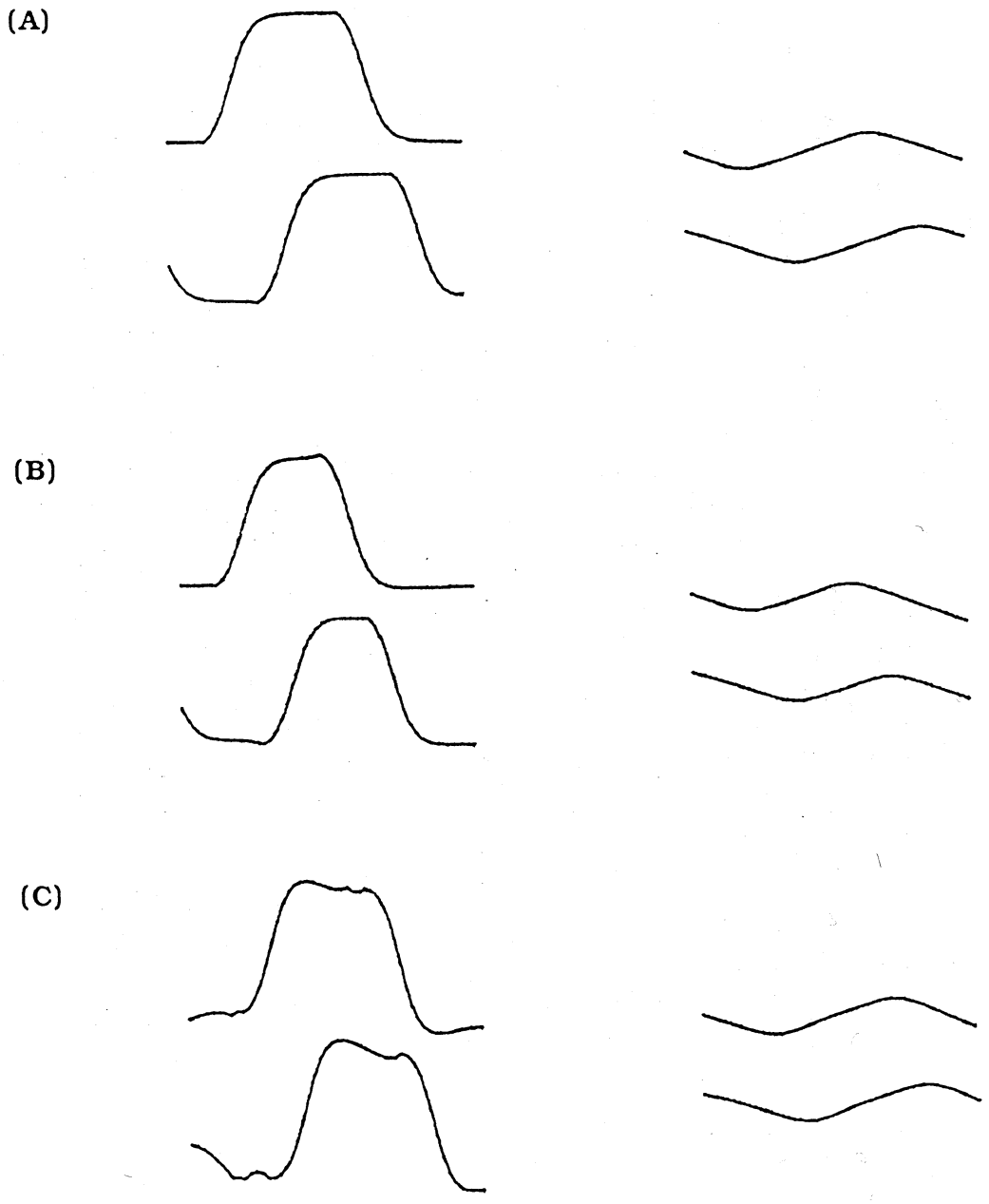

Fig.4

(A)

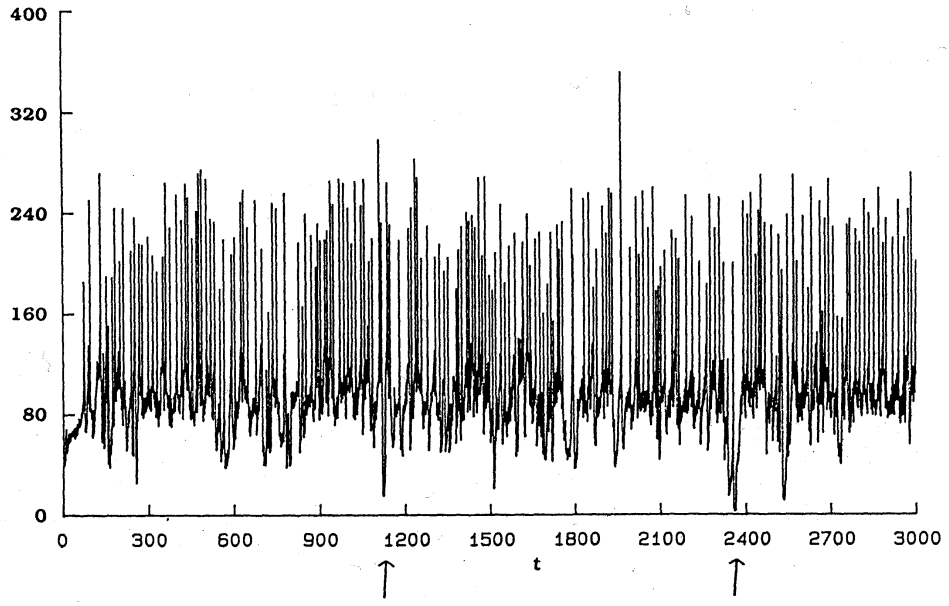
400
320
240
160
80
0
0
300
600
900
1200
1500
1800
2100
2400
2700
3000
t

(B)

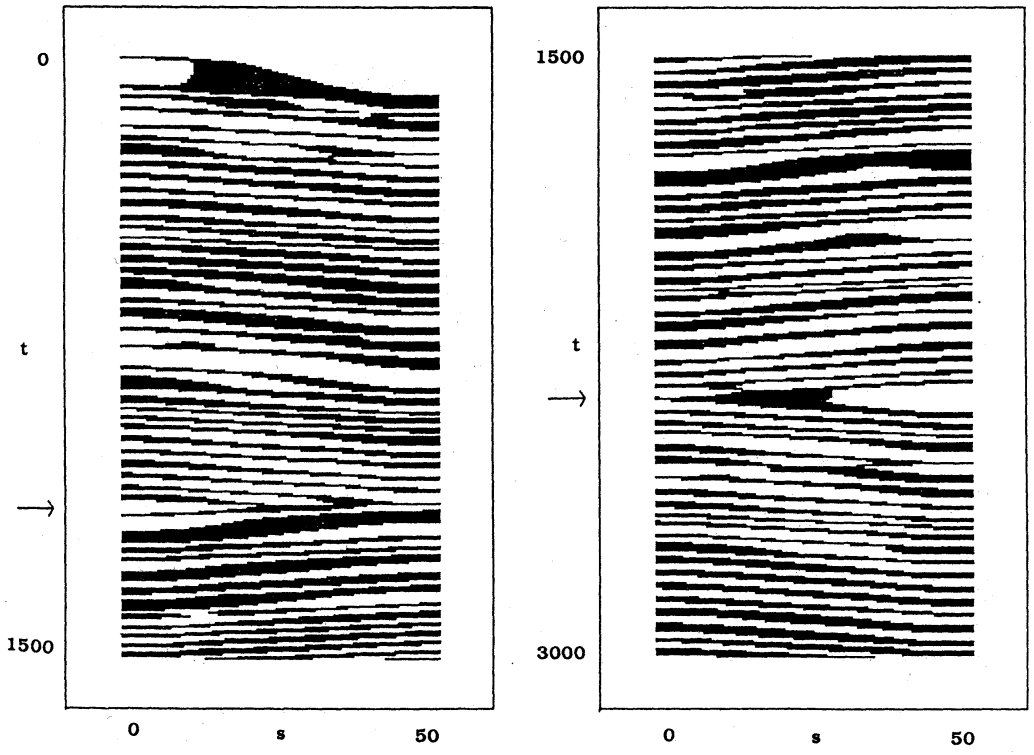
0
t
1500
0
s
50
1500
t
3000
0
s
50

Fig. 5

(A)

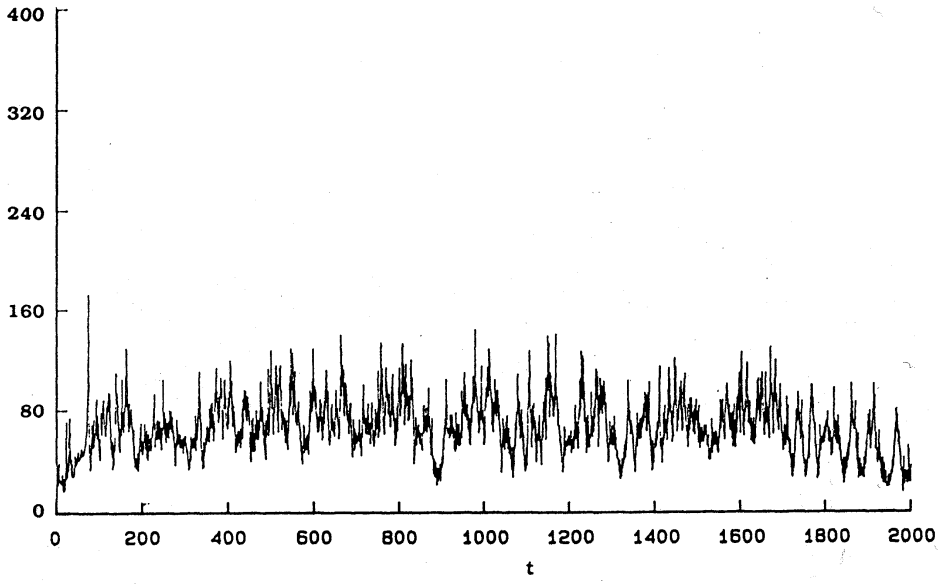
400
320
240
160
80
0
0
200
400
600
800
1000
1200
1400
1600
1800
2000
t

(B)

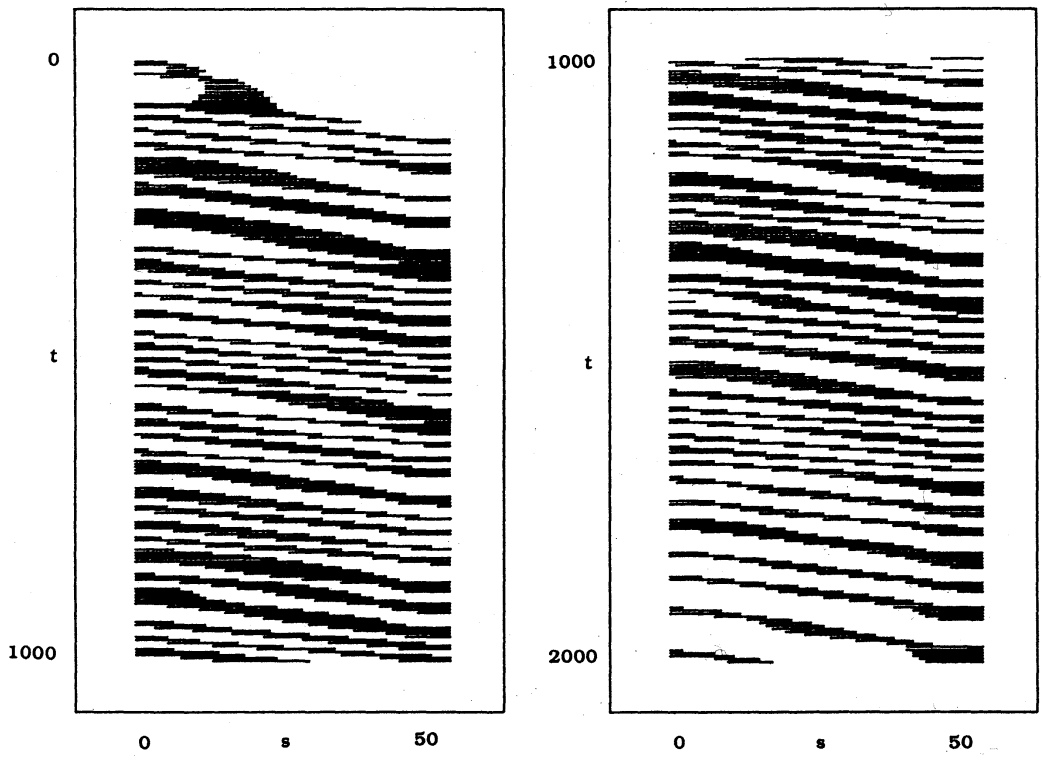
0
t
1000
0
s
50
1000
t
2000
0
s
50

Fig. 6

(A)

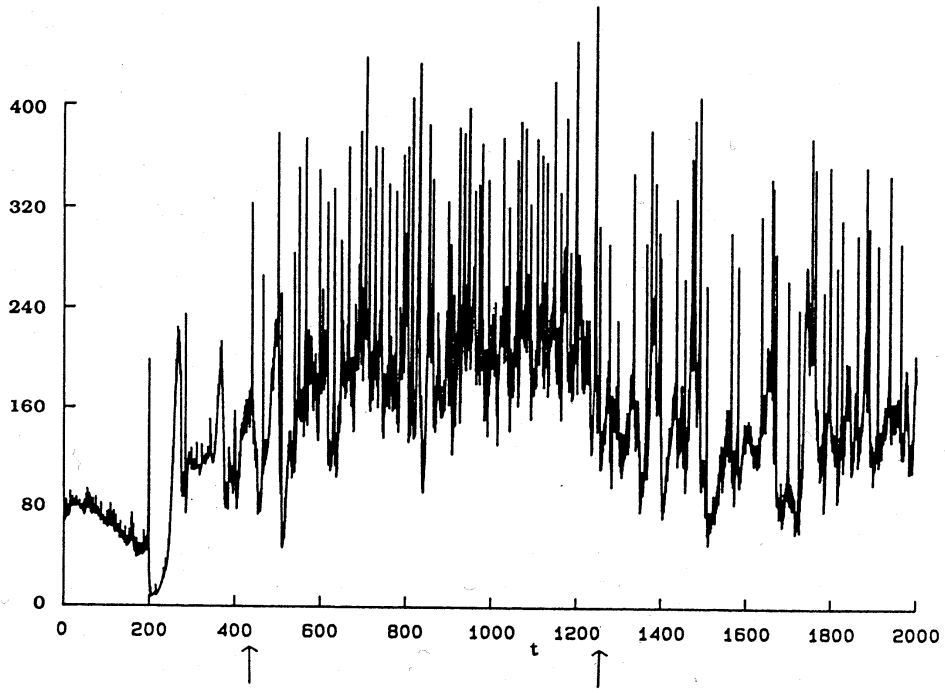
400
320
240
160
80
0
0
200
400
600
800
1000
1200
1400
1600
1800
2000
t

(B)

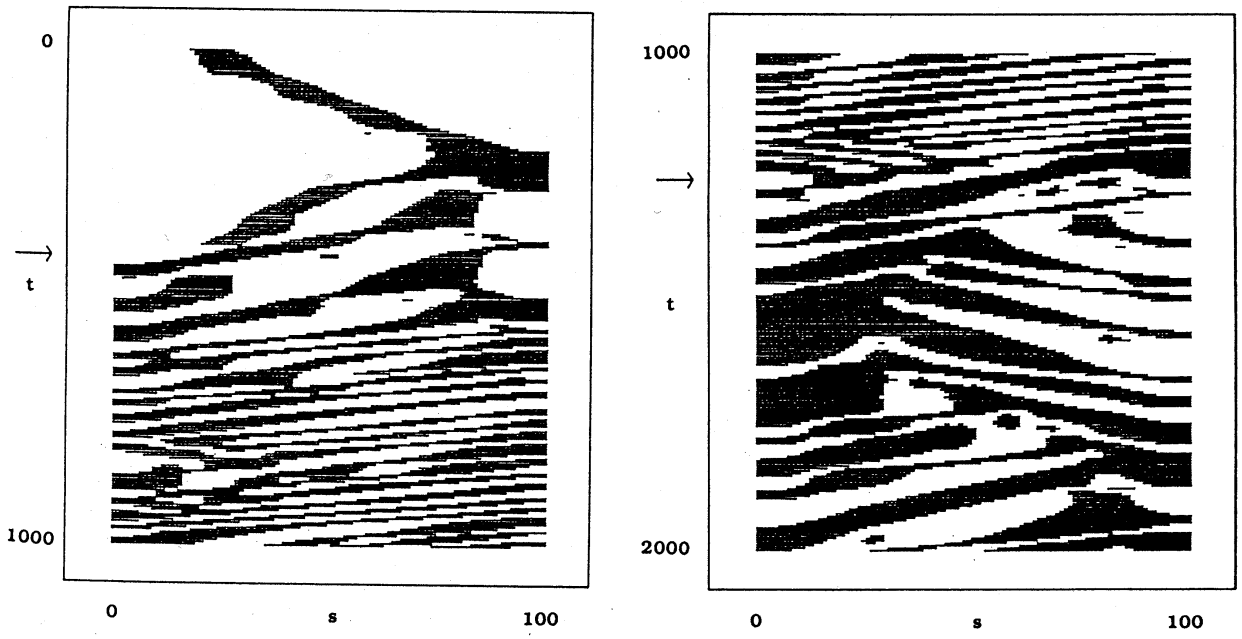
0
t
1000
0
s
100
1000
t
2000
0
s
100

Fig. 7